

Article

Experimental Study on External Loading Performance of Large Diameter Prestressed Concrete Cylinder Pipe

Pengran Shang ^{1,2} , Hao Wang ³, Di Zhang ², Wenkui Zheng ², Fulai Qu ^{2,*}  and Shunbo Zhao ^{1,2,*} 

¹ Collaborative Innovation Center for Efficient Utilization of Water Resources, North China University of Water Resources and Electric Power, Zhengzhou 450046, China

² International Joint Research Lab for Eco-Building Materials and Engineering of Henan, Zhengzhou 450045, China

³ Henan Fuchen Pipe Co., Ltd., Xinxiang 453400, China

* Correspondence: qfl@ncwu.edu.cn (F.Q.); sbzhao@ncwu.edu.cn (S.Z.)

Abstract: A prestressed concrete cylinder pipe (PCCP) is created with a complex composition of concrete core, welded steel cylinder, prestressed steel wire, protective mortar and anti-corrosion coating. Due to the economy and complexity of structural prototype tests, the ultimate loading test on PCCP is rarely conducted. In this paper, the three-edge bearing test was carried out on a 3.2 m diameter PCCP with embedded steel cylinder. The strains of concrete core, prestressed steel wire and protective mortar were monitored, and the distribution and width of the concrete cracks were recorded. The test results show that the cracking on the inside concrete at the crown zone occurred before those on the invert zone of the pipe. The prestressed steel wire postponed the tensile stress of out-side concrete at the springing line until subjected to the calculated cracking load (P_c). Due to the moment redistribution caused by the cracking on the inside of the concrete at the crown/invert, the protective mortar at the springing line was cracked at $1.2 P_c$ and exhibited visible cracking after $1.4 P_c$. The prestressed steel wire reached the elastic and strength limit states of $1.4 P_c$ and $1.6 P_c$, respectively. The PCCP designed by the limit state design method can resist the increased external loads after reaching the serviceability limit state. The final failure load of the test pipe is greater than $1.6 P_c$, and there is sufficient safety in actual operation. Due to the fact that the damage to the concrete at the crown/invert zone may become a fuse of PCCP failure, the tensile stress of the inside concrete at the crown/invert zone of the PCCP should be accurately verified in the design process.

Keywords: prestressed concrete cylinder pipe (PCCP); external pressure; three-edge bearing test; crack; strain; deformation; limit state



Citation: Shang, P.; Wang, H.; Zhang, D.; Zheng, W.; Qu, F.; Zhao, S. Experimental Study on External Loading Performance of Large Diameter Prestressed Concrete Cylinder Pipe. *Buildings* **2022**, *12*, 1740. <https://doi.org/10.3390/buildings12101740>

Academic Editors: Hongyuan Fang, Baosong Ma, Qunfang Hu, Xin Feng, Niannian Wang, Cong Zeng and Hongfang Lu

Received: 17 September 2022

Accepted: 18 October 2022

Published: 19 October 2022

Publisher's Note: MDPI stays neutral with regard to jurisdictional claims in published maps and institutional affiliations.



Copyright: © 2022 by the authors. Licensee MDPI, Basel, Switzerland. This article is an open access article distributed under the terms and conditions of the Creative Commons Attribution (CC BY) license (<https://creativecommons.org/licenses/by/4.0/>).

1. Introduction

To ensure that the deformation of the concrete pipe under the working pressure or external load does not exceed the allowable elongation strain, certain induced stress can be applied to the core concrete to greatly increase its tensile resistance [1]. The amount of steel used for the pipe can be reduced while bearing high working pressure. Hence, the prestressed concrete cylinder pipe (PCCP) was created by the combination of conventional reinforced concrete pipe and prestressed technology. PCCP consists of a concrete core, prestressed steel wire, protective mortar coating and anti-corrosion coating. The pipe core is composed of a thin steel plate and concrete, of which the thin steel plate is continuously rolled and welded into a cylinder. The core concrete is formed by centrifuging inside the steel cylinder or simultaneously vertically pouring inside and outside the steel cylinder. According to the arranged position of the steel cylinder, PCCP can be divided into lining type and embedded type. Figure 1 shows the composition of the embedded type. The diameter is 0.4~1.6 mm for the lining type, and 0.6~4.0 m for the embedded type [2,3].

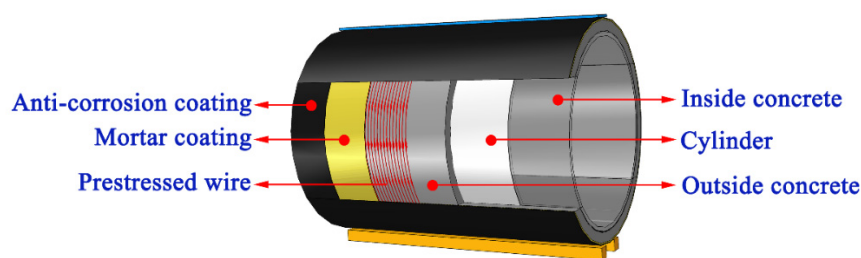


Figure 1. Schematic diagram of the composition of embedded PCCP.

Due to the advantages of high working pressure, good impermeability and durability as well as plant production and convenient installation, PCCP has been widely used in the transmission and distribution of water in municipal, industrial and irrigation systems [3]. North America has PCCP pipelines over 35,000 km long [4]. With the development and maturity of PCCP technology, China has PCCP pipelines over 30,000 km long [5–7]. Moreover, other countries in North Africa also use PCCP for water conveyance projects. Typical engineering practices include the Great Man-Made River in Libya and the Chinese South-to-North Water Diversion Project [8].

The early design method of PCCP mainly controls the water pressure with the ultimate tensile strength of concrete by using the allowable stress method [9]. A multi-layer ring model for PCCP structural analysis is proposed by Zarghamee based on hundreds of summarized and analyzed groups of pressure pipe test data [10,11]. Subsequently, Zarghamee and Herge [12,13] proposed a limit state design method based on the principle of mathematical statistics, which provides a basis for the specification of code ANSI/AWWA C304 [3]. In addition, China has gradually formed the limit state design methods specified in codes CECS 140 [14] and SL 702 [15] with the continuous investigation in the field of PCCP.

During its service life, PCCP is required to endure certain external loads such as soil covering and vehicles. Generally, the three-edge bearing test can be used to evaluate the bending characteristics and mechanical response of the PCCP under external loads. With more than 200 sets of three-edge bearing test results of PCCPs summarized by Zarghamee [10], including the load data of the first visible crack, the crack with a width of 0.25 mm and the ultimate strength, the limit state design method has been verified to be very conservative. To evaluate the external load performance of the PCCP designed by the limit state design method, Dou and Hu [16–18] conducted three-edge bearing tests on the PCCP with pipe diameters of 2.6 m and 4.0 m. However, due to the loading of these studies being limited in the serviceability of the PCCPs, the mechanical response of the PCCPs after cracking could not be evaluated. Zhao [19] provided the crack development of the pipe body under overload compression by conducting an overload test on the embedded PCCP with a pipe diameter of 4.0 m. Unfortunately, this experiment did not collect the deformation data of the pipe barrel.

The failure study on PCCP tends to use finite-element software for numerical analysis due to the limitations in test design and equipment [20,21]. Currently, a technology of pipe with broken wires strengthened by prestressed CFRP has been developed to repair PCCPs that are in or about to be in a failure state [8,22]. The difficulty of using the technologies lies on the evaluation of the PCCP's condition. The previous monitoring methods could not monitor the corrosion of the bell and spigot ring of PCCP well [4,23]. A novel corrosion monitoring method for PCCP spigots that combines the Tafel extrapolation and surface acoustic wave methods was recently proposed by Wang et al. [24]. The adverse effect of strike-slip fault displacement and uneven settlement of foundation on the spigot and bell ring of burial PCCP was studied by Li [25] and Wu [26], respectively. In addition, PCCP is easy to be eroded by corrosive medium under a buried environment [27]. The use of a pozzolanic material will make PCCP more durable under harsh conditions [28,29].

Currently, the three-edge bearing test is inclined toward structural identification at the serviceability limit states. This is adaptable to evaluate whether the products of manufactured PCCPs satisfies the design regulations, and to verify whether the pipe's

concrete cracks or exhibits visible cracks. Generally, the theoretical cracking load of the PCCP is deduced by the prestressed and classical mechanics. However, the economy of PCCP with a diameter larger than 2.0 m is a major advantage as a water transmission trunk line. When underground PCCP fails due to management's improper operation, power failure and other accidental circumstances, the design characteristics of a large diameter will lead to unimaginable consequences [30]. Once these consequences occur, existing knowledge may not well explain the failure behavior of the PCCP. This requires further studies on the mechanical properties of PCCP under conditions that exceed the normal serviceability.

In this paper, combined with practical engineering, a three-edge bearing test is carried out on the full-scale embedded PCCP with a diameter of 3.2 m. The tested PCCP is designed according to the limit state design method of codes CECS 140 [24] and AWWA C304 [3]. During the test, the strain of core concrete, prestressed steel wire and protective mortar were measured, and the crack width and crack distribution were observed and recorded. In addition, the deformation of various stages of the PCCP under external loads were detected in combination with the control criteria at the corresponding limit state. This experiment is part of a research project on PCCP technology innovation. The purpose of this study is to understand the performance of the current PCCP structure. Moreover, it can also help designers better master the limit state design method.

2. Experimental Work

2.1. Manufacturing of Tested PCCP

An embedded type of PCCP, single-layer and wrapped with prestressed steel wire, was used in the test. The PCCP was designed according to codes CECS 140 [14] and AWWA C304 [3] and manufactured according to codes GB/T 19,685 [2] and AWWA C301 [31]. The structural composition is shown in Figure 2, and the geometrical sizes are listed in Table 1. In accordance with the specifications of the codes [32–34], the core concrete and the protective mortar were designed at strength grades of C55 and M45, respectively, with a cubic compressive strength of 55.0 MPa and 45.0 MPa; the prestressed steel wire was designed at a strength grade of 1570 MPa, and the thin steel plate for the steel cylinder was designed at a strength grade of 300 MPa.

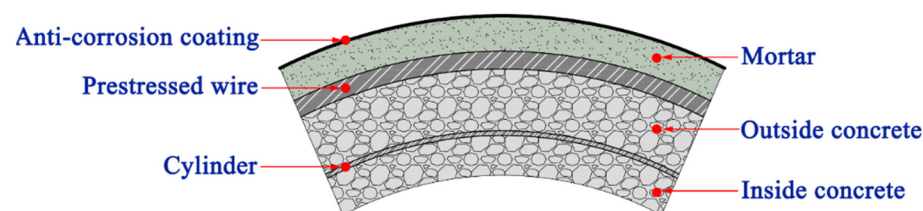


Figure 2. Schematic diagram of structural section composition.

Table 1. Geometry and design parameters for tested PCCP.

Internal Diameter (mm)	Working Pressure (MPa)	Underground Burial Depth (m)	Thickness of Core Concrete * (mm)	Thickness of Protective Mortar (mm)	Thickness of Steel Cylinder (mm)	Wire Diameter (mm)	External Diameter of Steel Cylinder (mm)	Gross Wrapping Stress (MPa)	Wire Area (mm ² /m)
3200	0.4	5	245	25	1.5	7	3343	1099	2350

Note: * The thickness of core concrete includes the thickness of inner wall concrete, outer wall concrete and steel cylinder.

The steel cylinder of the PCCP was continuously welded with the thin steel plate, and the bell and spigot steel rings were welded at the ends of the steel cylinder. It was vertically installed in the steel mold and embedded by the inside and outside core concrete to form the pipe core. The core concrete was poured into the steel mold as it was made to vibrate. Steam curing technology was used to cure the pipe core concrete to reach 70% of the design

strength. After that, the steel mold was demolded, the prestressed steel wire was wrapped and the protective mortar was roll-sprayed to form a dense protective layer. Finally, the solvent-free epoxy coal tar pitch was used to make anti-corrosion coating and ensure the anti-corrosion of the bell and spigot steel ring. The manufacturing process for testing PCCP is shown in Figure 3.



Figure 3. The manufacture process of PCCP: (a) Welded steel cylinder; (b) Pouring of concrete; (c) Concrete core; (d) Wrapping of prestressed steel wire; (e) Roll shooting of protective mortar; (f) Anti-corrosion coating.

When testing for the PCCP, the pipe concrete and protective mortar were, respectively, at 91 days and 86 days of age with the respective measured compressive strengths of 65.6 MPa and 48.2 MPa. Combined with the specifications in the codes [32–34], the mechanical properties of the materials for the tested PCCP are presented in Table 2.

Table 2. Material properties of tested PCCP.

Material	Compressive Strength (MPa)	Modulus of Elasticity (MPa)	Tensile Strength (MPa)	Yield Strength (MPa)
Concrete	65.6 *	35,500	2.74	/
Mortar	48.2 *	24,165	3.49	/
Cylinder	/	206,000	470 *	300 *
Prestressed wire	/	205,000	1620 *	1177.5

Note: * Test values, others are determined as per Chinese codes [32,33].

2.2. Monitoring Point Arrangement and Test Equipment

2.2.1. Monitoring Point Arrangement

Three Sections 1–3 were set along the axis of the test pipe, as shown in Figure 4. Four circumferential strain gauges were arranged at 90° intervals on each section of the inner wall of the pipe, while a dense arrangement at 45° and 135° and their symmetrical positions were made in the middle of Section 2. The strain gauges on the outside of the pipe were symmetrically arranged at the sides of the springing line. One side was grooved to exclude the anti-corrosion coating and protective mortar, while the strain gauges were pasted on the exposed steel wire and the outer surface of the concrete. Another side was made to expose the protective mortar, while the strain gauges were pasted to monitor the mortar strain. Two mortar monitoring areas were densified at 135° and 225° in the middle of Section 2. A total of 26 measuring areas and 34 measuring points were set on the pipe. Meanwhile, the displacement meters with a range of 50 mm were set near the bell and spigot ring ends to monitor the vertical displacement of the pipe's crown.

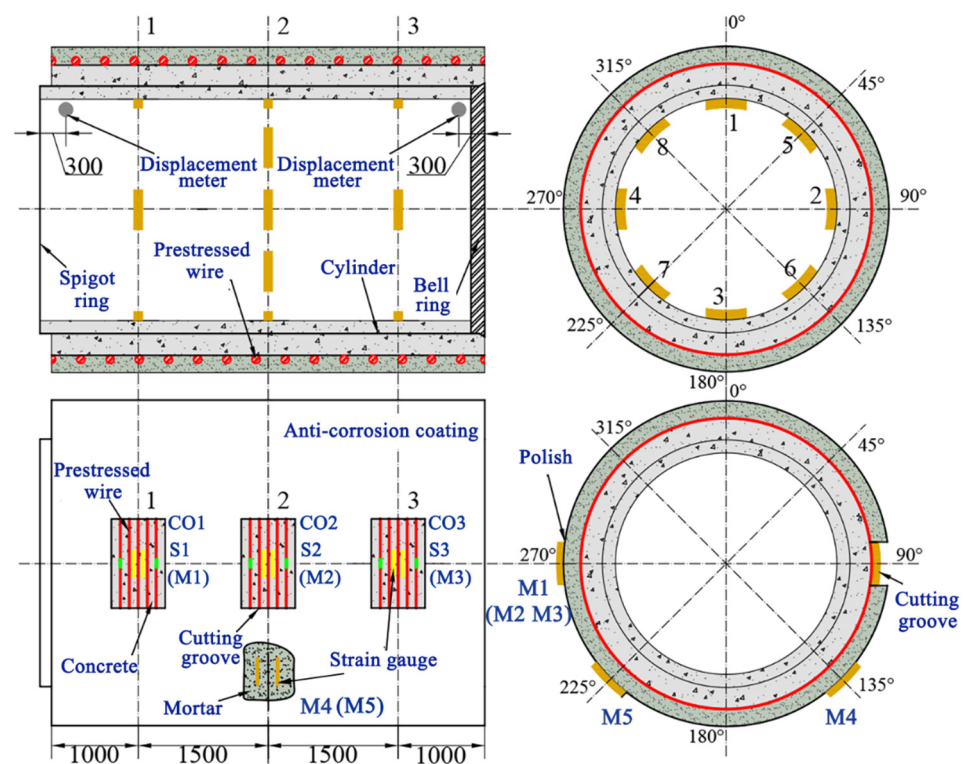


Figure 4. Schematic diagram of monitoring point arrangement (unit: mm).

The concrete measuring points on the inner and outer surfaces of the pipe were identified as Cl_{i-j} and Co_i , respectively, and those on the steel wire and protective mortar were numbered in the form of Si and Mi , respectively, where i and j represent the section and measuring point numbers, respectively.

2.2.2. Monitoring Instruments

The strain gauges used for the concrete, the prestressed steel wire and the mortar are of the resistance type. The strain gages for the concrete and the mortar are paper-based with a gauge length of 100 mm, and the measured resistance is (119.5~119.9) Ω . The strain gauge for the prestressed steel wire is rubber-based with a length of 3 mm, and the measured resistance is (120.1~120.5) Ω . Before pasting, the surface of the monitoring point was polished and cleaned with absolute ethanol. The epoxy resin was used to make a base and paste the strain gauges immediately. Finally, a layer of plastic film was covered on the pasted strain gauge for moisture-proof treatment. The curing time of the epoxy resin was of no less than 24 h, as shown in Figure 5a–c.

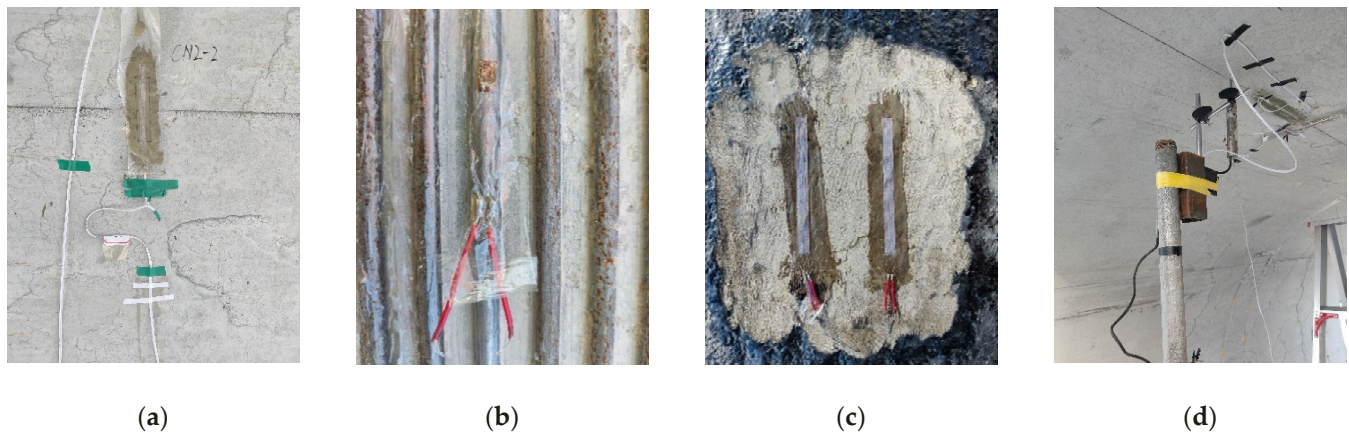


Figure 5. Strain gauge and displacement meter: (a) Concrete; (b) Prestressed steel wire; (c) Mortar; (d) Displacement meter.

The displacement meter, with an accuracy of 0.001 mm, was used to collect pipe crown displacement data, fixed by a special support frame as shown in Figure 5d.

The Donghua Static DH3821 high-speed static strain measurement system was used to collect the strain of PCCP, as shown in Figure 6. The strain gauge was connected to the signal input line through the wire by the Wheatstone bridge. Each collector has 16 channels. Three collectors with a total of 48 channels were used in the test. This fully meets the needs of the measuring points.

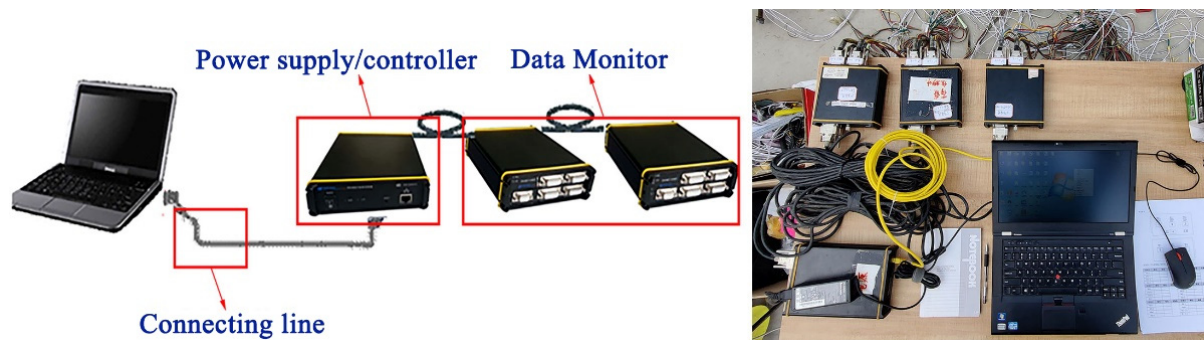


Figure 6. Static DH3821 high-speed static strain measurement and analysis system.

2.2.3. Load Device

The external pressure load testing machine produced by Jiangsu Bangwei Machinery Manufacturing Co., Ltd., Yangzhou, China, was used in this test. It can be applied to the test of PCCP with a pipe diameter of 0.6~3.5 m and a length of no more than 6.0 m. As shown in Figure 7, the equipment is mainly composed of an upper steel beam, and the steel frame with an invert beam, four columns and a rigid steel foundation. Six hydraulic jacks fixed on the inverted beam are simultaneously actuated by an oil pump and push the upper steel beam to exert a uniform load along the top surface of the pipe. The upper steel beam can freely be slid along the vertical chute of the columns. A rubber cushion 40 mm-thick is placed between the top of the pipe and the steel beam. Two hardwood beams placed on the foundation are used as the supports of the test pipe. The displayed value of the machine terminal computer is the total pressure of the six jacks. The actual load acting on the test pipe is the sum of the measured and the weight of the top steel beam.

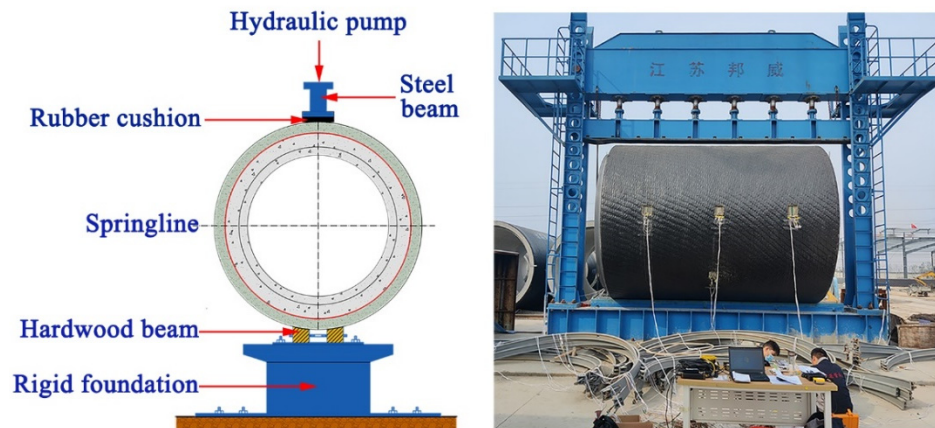


Figure 7. Schematic diagram of the load device.

2.3. Calculation of Load and Control Strain

2.3.1. Final Prestress of Prestressed Steel Wire

The final prestress σ_{pe} of the circumferential steel wire is equal to the gross wrapping stress σ_{con} of the wire minus the prestress loss, which is calculated by the Formula (1):

$$\sigma_{pe} = \sigma_{con}(1 - 0.08\phi_t\phi - 0.5n_s\rho_y) - \sigma_{s3} \quad (1)$$

where ϕ_t is the influence coefficient of the manufacturing process of the pipe's core, which is 1.0 for embedded PCCP; ϕ is the reinforcement influence coefficient, which is 1.0 for single-layer wrapping; ρ_y is the reinforcement ratio of prestressed wire, %.

The prestress loss σ_{s3} caused by concrete shrinkage and creep is determined by the ratio of the normal precompression stress σ_p on the pipe wall section to the standard value f'_{cu} of concrete cube compressive strength when prestress is applied. To ensure the convergence of concrete shrinkage and creep, $\sigma_p \leq 0.5f'_{cu}$ is specified [14]. For single-layer wrapping, σ_p is calculated by Formula (2). Finally, σ_{s3} is obtained from Table 3.

$$\sigma_p = \frac{A_p\sigma_{con}}{1000t + (n_y - 1)1000t_y + n_sA_p} \quad (2)$$

where A_p is the sectional area of prestressed steel wire, mm^2/m ; n_s is the ratio of the modulus of elasticity between wire and concrete; n_y is the ratio of the modulus of elasticity between steel cylinder and concrete; t_y is the thickness of steel cylinder, mm; t is the thickness of the pipe core (including the thickness of the steel cylinder), mm.

Table 3. Prestress loss caused by concrete shrinkage and creep.

σ_p/f'_{cu}	0.1	0.2	0.3	0.4	0.5
σ_{s3} (MPa)	20	30	40	50	60

2.3.2. Conversion Coefficient of Tensile Edge Resistance Moment of the Inner Wall

Due to the nonuniformity of PCCP materials, the elastic resistance moment of a single material cannot be directly calculated, and the reduction coefficient of a resistance moment ω_c needs to be determined. It can be calculated as follows:

$$\omega_c = \frac{6(I_c + I_y + I_s + I_m)A_n}{1000S_nT^2} \quad (3)$$

where I_c , I_y , I_s and I_m are the inertia moment of the converted section of concrete, steel cylinder, prestressed wire and mortar to the centroidal axis of the converted section, respectively, mm^4 ; S_n is the converted area moment of the pipe core concrete, steel cylinder,

prestressed wire and mortar section to the inner surface of the pipe wall, mm^3/m ; A_n is the converted area of the section of pipe core concrete, steel cylinder, prestressed wire and mortar, mm^2/m ; T is the pipe wall thickness, mm.

2.3.3. Calculation of Theoretical Cracking Load

The theoretical cracking load (P_c) refers to the load corresponding to the onset of visible cracks (width greater than 0.05 mm) in the pipe barrel, which is calculated as follows [2]:

$$P_c = \frac{1.834\omega_c t^2 (A_p \sigma_{pe} / A_n + \alpha f_{tk}) L}{D_0 + t} \quad (4)$$

where α is the control cracking coefficient of the mortar; f_{tk} is the standard value of tensile strength, following China code GB 50,010 [33]; L is the actual length; D_0 is the nominal inner diameter of the pipe, mm. The result of P_c is presented in Table 4.

Table 4. Calculation results of P_c .

D_0 (mm)	t (mm)	σ_{pe} (MPa)	A_p (mm^2/m)	A_n (mm^2)	f_{tk} (MPa)	L (mm)	ω_c	P_c (kN)
3200	245	945.4	2350	285,959	2.74	4970	1.024	1735

2.3.4. Control Strain at the Limit State

The control strain was calculated based on the control criteria of limit state in codes AWWA C304 [3] and CECS 140 [14]. During the loading process, the pipe core concrete must first release the pre-compression caused by prestressing before tensile stress appears [18]. Therefore, the pre-compression strain (ε_{c0}) of concrete and actual prestress after deducting prestress loss shall be calculated to modify the control strain of concrete and prestressed wire. The results are listed in Table 5. It is worth noting that microcracking corresponds to 0.025 mm-wide cracks, and visible cracking corresponds to 0.05 mm-wide cracks.

Table 5. Calculation results of the control strain.

Limit State	Parameter	Position	Meaning	Control Criteria	Strain ($\mu\varepsilon$)
Serviceability	ε_{c0}	Invert/Crown	Pre-compression strain of concrete	/	-235^1
	ε_{ce}		Elastic strain of concrete	/	312
	ε_{ctm}		Microcracking on concrete	$1.5\varepsilon_{ce}$	351
	ε_{ctv}		Visible cracking on concrete	$11\varepsilon_{ce}$	1082
	ε_{fci}	Springing line	Compression strain of concrete	$0.55f_c'^2$	-550
	ε_{me}		Elastic strain of mortar	/	144
	ε_{mt}		Theoretically cracking strain of mortar	$4\varepsilon_{me}$	576
	ε_{mtm}		Micro cracking on mortar	$6.4\varepsilon_{me}$	922
	ε_{mtv}		Visible cracking on mortar	$8\varepsilon_{me}$	1152
	Elastic	ε_{fci}	Springing line	Compression strain of concrete	$0.75f_c'$
ε_{wt}		Springing line	Wire strain corresponding to gross wrapping stress	$\sigma_{wt} \leq \sigma_{con}$	748
Strength	ε_{wy}	Springing line	Wire strain corresponding to yield stress	$\sigma_{wt} \leq f_{sy}$	1132

Note: ¹. “-” represents compression; ². f_c' represents the standard value of axial compressive strength.

2.4. Test Process and Method

The test was conducted according to codes GB/T 15,345 [35] and ASTM C497 [36]. The tested PCCP was transported to the external pressure equipment by the double girder gantry crane. Two hard straight wooden beams with a length of 6.0 m and with a square section of 150 mm were set as the supports. The surface of the beams in contact with the

pipe was treated as an arc with a radius of 13 mm. The clear spacing of the inner non-arc area is 1/12 of the outer diameter of the test pipe, that is, 312.8 mm.

The load was exerted step-by-step at 10% P_c , which was calculated by the Formula (4). The loading speed in the test was controlled at 30~50 kN/m. Each step load was held for 1 min before it reached 80% P_c , 3 min when it was at (90~100%) P_c and 5 min when it was above 100% P_c . At the end of each holding time, the cracking condition of the tested PCCP was observed and the strain data were recorded. After cracking, the width and distribution zone of the cracks were measured and recorded at the same time. The crack width is measured by a crack observer with an accuracy of 0.02 mm, as shown in Figure 8.



Figure 8. Crack observation instrument.

3. Width and Distribution of Concrete Cracks

Based on the test, the pipe did not crack before the load reached 100% P_c . When loaded to 100% P_c , two longitudinal cracks appeared on the pipe's crown: one was 2 m apart from the bell ring end, 0.02 mm wide and 250 mm long; another was 3.6 m apart from the spigot ring end, 0.04 mm wide and 150 mm long. When the load continuously increased to 110% P_c , seven new longitudinal cracks with a maximum width of 0.10 mm appeared on the pipe's crown, and the first two original cracks expanded to a width of 0.08 mm. The first crack at the pipe invert was 0.06 mm wide. At 120% P_c , there were five new longitudinal cracks on the pipe's crown, the maximum width was 0.12 mm and the maximum width of the cracks appeared earlier was 0.22 mm. A new longitudinal crack with a width of 0.10 mm appeared at the pipe invert, and the first crack to appear expanded to 0.12 mm. At 130% P_c , no newer crack appeared on the pipe's crown. The existing cracks expanded over 0.2 mm, and the maximum width was 0.34 mm. Three new longitudinal cracks with a maximum width of 0.22 mm appeared at the pipe invert, and the existing cracks expanded to 0.28 mm. The crack distribution and width are shown in Figure 9 and Table 6.

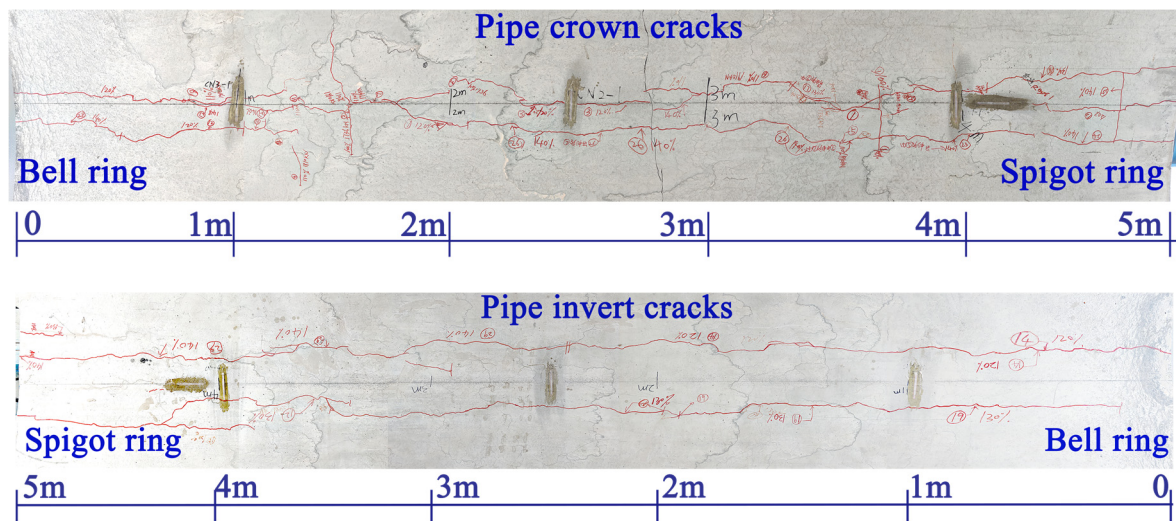


Figure 9. Diagram for distribution zone of cracks on the inner surface of pipe concrete.

Table 6. The width and distribution zone of concrete cracks.

Crack No. ¹	Distribution Zone	Crack Width (mm) ²				
		100% P_c (1736 kN)	110% P_c (1910 kN)	120% P_c (2083 kN)	130% P_c (2257 kN)	
1	Crown	0.04	0.08	0.22	0.34	
3		0.02	0.08	0.10	0.26	
4		/ ³	0.08	0.12	0.32	
5		/	0.06	0.08	0.20	
6		/	0.06	0.16	0.26	
7		/	0.04	0.18	0.30	
8		/	0.10	0.22	0.34	
10		/	0.10	0.14	0.30	
11		/	0.08	0.20	0.28	
12		/	/	0.06	0.26	
13		/	/	0.10	0.22	
16		/	/	0.12	0.26	
17		/	/	0.08	0.22	
18		/	/	0.10	0.26	
14		Invert	0.02	0.06	0.12	0.28
15			/	/	0.10	0.28
19			/	/	/	0.16
20			/	/	/	0.22
21	/		/	/	0.14	

Note: ¹. The missing number is the circumferential crack; ². The width of cracks after 140% load was not observed; ³. "/" represents that there is no crack under the current load.

It can be seen from Figure 9 that the cracks at the pipe's crown zone are distributed along the axis and nearby, while the cracks at the invert zone of the pipe are approximately uniformly distributed along both sides of the axis. According to the results of the measurement, the cracks at the invert zone are distributed within the distance between the two hard straight wooden beams. The difference between the distribution of the cracks on the crown and invert zones was caused by the support conditions at the invert.

There is no evident law for the appearance of cracks at the initial stage of cracking. At first, micro cracks appeared randomly. With the increase in load, the number and width of the cracks increased, and each crack gradually connected. When the load reached 130% P_c , the width of many cracks exceeded 0.25 mm. Therefore, for the safety of operation, the crack width was not observed when load reached 140% P_c and subsequent much higher loads. The test results show that the cracking of the pipe's crown zone occurred earlier

than that of the invert. However, when the load reached 130% P_c , the cracks at the crown and invert zones of the pipe connected and the width of the cracks exceeded 0.25 mm.

4. The Monitoring Result of Strains

4.1. Concrete Strain

4.1.1. Crown and Invert (0° and 180°) zones of Pipe

The load-strain relationships of the pipe's concrete at the crown and invert inner surface are shown in Figure 10a,b. The concrete at the crown reached the decompression point at 70~80% P_c , the theoretical elastic limit at 90% P_c and the micro cracking control strain at 90~100% P_c . The decompression point means the pre-compression stress in the concrete core drops to zero. The concrete at the pipe's invert zone reached the decompression point at 80% P_c , the theoretical elastic limit at 90~100% P_c and the micro cracking control strain at 100% P_c . The visible crack control strain was reached in the crown and invert inner surfaces of the pipe at the loading of 110~120% P_c and 120~130% P_c , respectively. When the load reached 130% P_c , the strain gauges at all monitoring points on the crown of the pipe were damaged. Differing from the crown of the pipe, the crack position at the invert of the pipe was outside the gauge length of the strain gauge at the monitoring point, except for CI1-3. The strain curve shows a downward trend due to the strain release of the crack. The test results show that in front of the invert zone, the crown zone of the inner concrete first reached the visible crack control strain.

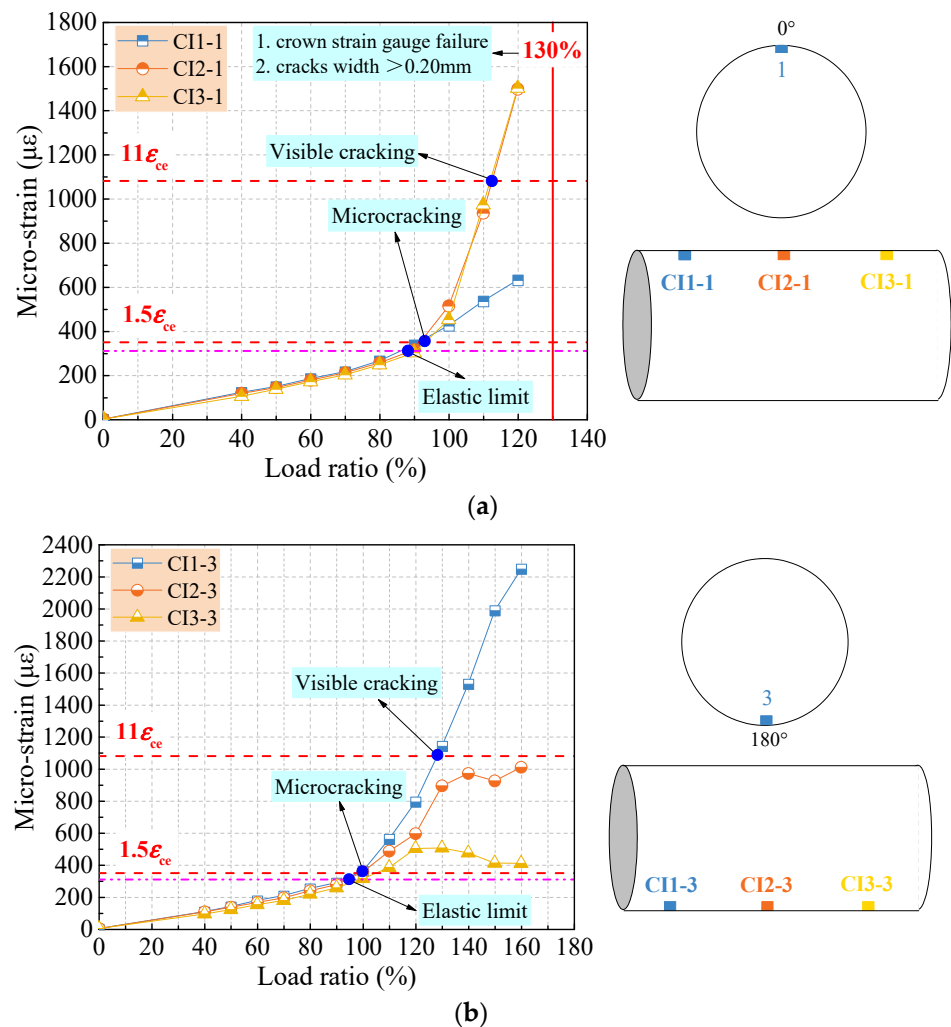


Figure 10. The load-strain relationships of the concrete at: (a) Crown (0°); (b) Invert (180°).

4.1.2. Springing line (90° and 270°)

The load-strain relationship of the concrete on the inner and outer surfaces at the springing line of the pipe are shown in Figure 11, where the negative of the Y axis represents the compressive strain. Evidently, the stress state of the inner concrete surface at the springing line of the pipe was in compression, while the outer concrete surface was in tension. This means that the concrete at the longitudinal section of the springing line produced a deformation from inner compression to outer tension. The outer concrete surface reached the decompression point at 100% P_c , the micro cracking control strain at 120% P_c and the visible crack control strain at 150%~160% P_c . The inner concrete surface reached the compressive stress control strain at 150% P_c . The test results show that the final strain of the inner concrete surface was lower than that of the outer concrete surface.

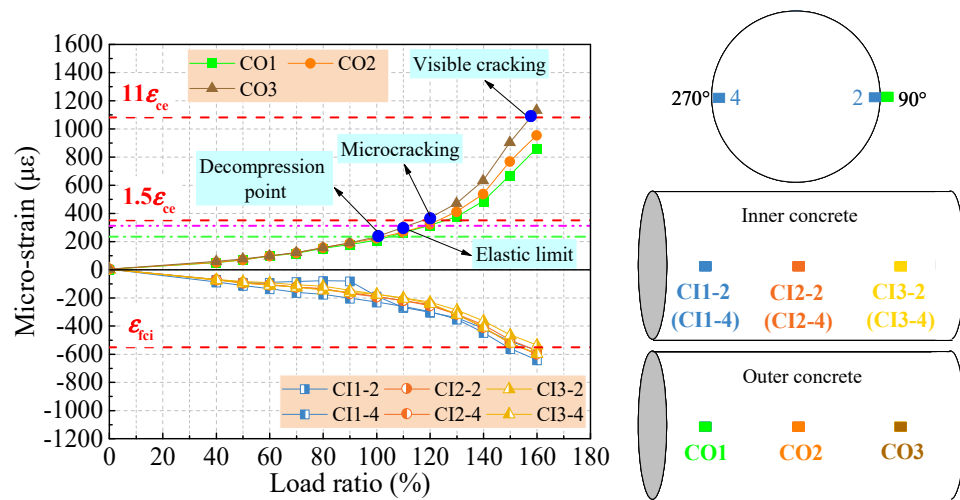


Figure 11. The load-strain relationship of the concrete at the springing line (90°, 270°).

4.1.3. Between Pipe Crown/Invert and Springing Line (45°, 135°, 225° and 315°)

The load-strain relationship of the inner concrete surface at 45°, 135°, 225° and 315° are shown in Figure 12. All monitoring points exhibit pressure characteristics. When loading to 120% P_c , the strain growth rate of each monitoring point increased and the final deformation was within 140 $\mu\epsilon$. The test results show that the inner concrete surface was in compression at 45°, 135°, 225° and 315°, and that the strain was far lesser than the concrete at the pipe’s crown, invert and springing line.

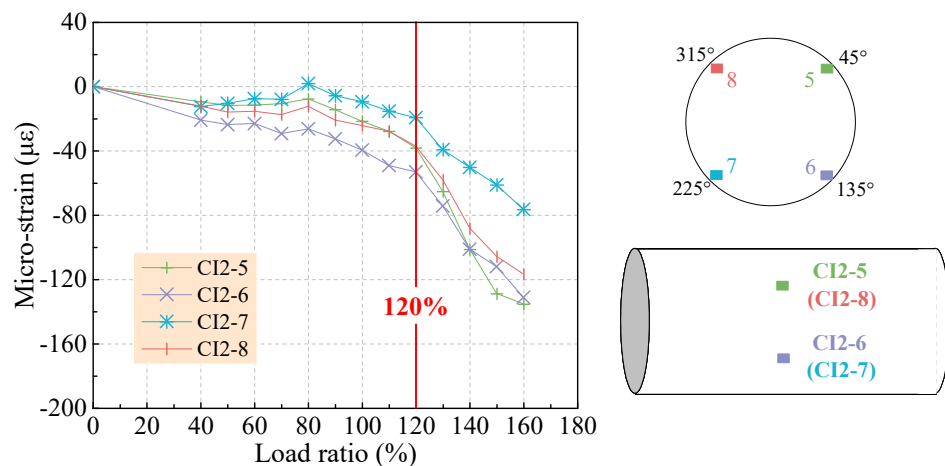


Figure 12. The load-strain relationship of the concrete between crown/invert and springing line (45°, 135°, 225° and 315°).

4.2. Prestressed Steel Wire Strain

The load-strain relationship of prestressed steel wire is shown in Figure 13. Before 100% P_c , the prestressed steel wire had a tensile strain below 300 $\mu\epsilon$, which was in the linear elastic stage. When the load reached 140%~150% P_c , the prestressed steel wire reached the gross wrapping stress, which was in the elastic limit state. When loading to 160% P_c , the steel wire reached a tensile strain of 1119 $\mu\epsilon$ (1175 MPa), which basically reached the strength limit state.

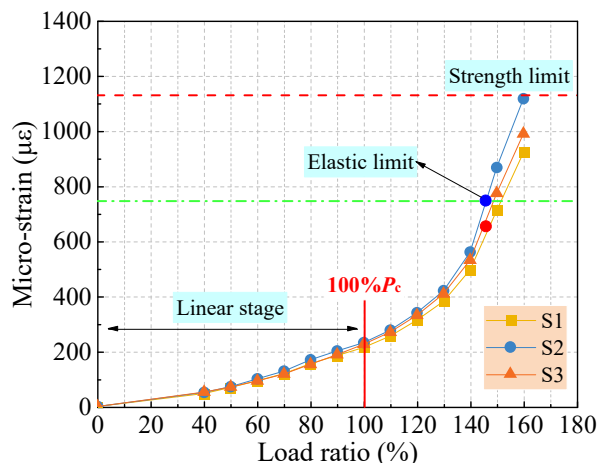


Figure 13. The load-strain relationship of the wire.

4.3. Protective Mortar Strain

The load-strain relationship of mortar for the tested pipe is shown in Figure 14. Before 100% P_c , the mortar strain was nearly 300 $\mu\epsilon$. When the load reached 120%~130% P_c , the mortar reached the initial crack state. When the load was continued to 140% P_c , the mortar reached the micro crack control strain. After 140% P_c , the mortar reached the visible crack control strain.

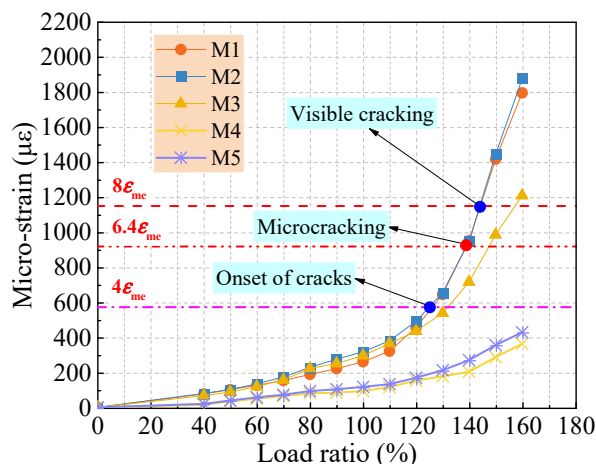


Figure 14. The load-strain relationship of the mortar.

The mortar remained in the elastic state at sections 135° and 225° with a tensile strain below 140 $\mu\epsilon$ before 110% P_c . The maximum strain was only 430 $\mu\epsilon$ even if the load reached to 160% P_c .

4.4. Displacement of Pipe Crown

The load-displacement relationship of the bell and spigot ring end at the pipe’s crown zone are shown in Figure 15. A good concordance between the displacement curves of the bell ring and the spigot ring was observed. The displacement of the pipe’s crown was of

7~8 mm at 100% P_c . When loading to 110% P_c , the pipe crown displacement was of about 10 mm. At 150% P_c , the prestressed steel wire reached the elastic limit state, and the pipe crown displacement was of 33~34 mm. The test results show that the displacement on the pipe's crown can reach as high as 40 mm under 160% P_c .

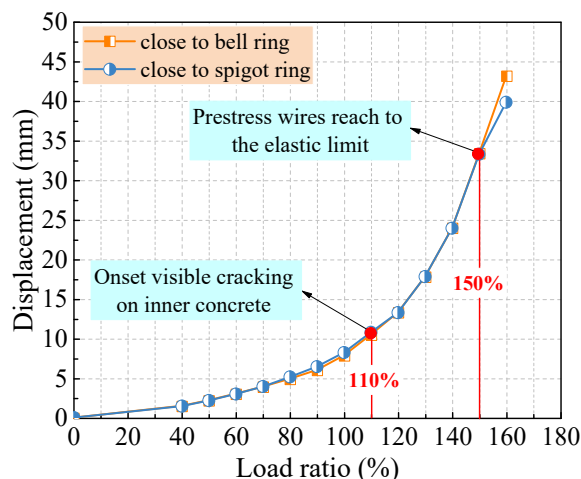


Figure 15. The displacement at the crown of the pipe changed with the load.

5. Discussion

5.1. Cracking Load for Concrete

The loads corresponding to the tensile parts of concrete at each stage are listed in Table 7. All the tensile parts of concrete are in a compression state before the load $0.7 P_c$ due to the existence of prestressing. The pipe's crown is first into the tensile state, and the concrete at the springing line remains in a prestressed state before the load P_c . The microcracking of concrete appears almost at the same time on the pipe's crown and invert zones under the load P_c . This indicates that the test results are consistent with the theoretical calculation results. For the load at visible cracking status, the test value ($1.1 P_c$) is lower than the theoretical calculation value ($1.2\sim 1.3 P_c$). This corresponds to the values of the control strain of visible cracks. The monitored value in the test was $9.5 \epsilon_{ce}$ ($970 \mu\epsilon$), which is lower than the value $11 \epsilon_{ce}$ ($1082 \mu\epsilon$) specified in the code AWWA C304 [3]. Therefore, different control strains of visible cracks may be obtained due to the change of the stress–strain relationship of concrete used for the calculation. Comparatively, the cracking of concrete at the outside of the springing line is posterior to that at the inside of the crown/invert zones. This is demonstrated by the fact that no cracking of concrete took place at the outside of the springing line under the load higher than 1.6 times that of the theoretical visible cracking. In this test, the crack width of concrete reaches 0.25 mm at the load $1.3 P_c$.

Table 7. Loads corresponding to different states of concrete.

Condition	Multiple of the Cracking Load P_c		
	Inside Concrete at the Crown	Inside Concrete at the Invert	Outside Concrete at the Springing Line
Decompression point	0.7~0.8	0.8	1.0
Elastic limit	0.8~0.9	0.9~1.0	1.1
Theoretically micro cracking	0.9~1.0	1.0	1.2
Experiment micro cracking	1.0	1.0	/
Theoretically visible cracking	1.2	1.2~1.3	1.5~1.6
Experiment visible cracking	1.1	1.1	/
The crack width to 0.25 mm	1.3	1.3	/

Under the pressure of external load, the stress state of concrete at the invert/crown zone is opposite to that at the springing line. That is, the tensile stress appears at the inside concrete of the invert/crown zone and the outside concrete of the springing line. In this test, the visible cracks appear on the inside concrete of the crown/invert zones when the load reaches $1.1P_c$, while the strain of the outside concrete along the springing line is still within $300 \mu\epsilon$. Therefore, the cracks will appear first on the inside concrete of the invert/crown zones of PCCP under the external load, while the cracking risk exists on the outside concrete of the springing line of the PCCP.

5.2. Stress State for Prestressed STEEL Wire

Combined with the cracking state of concrete and mortar, the stress state of the steel wire at each stage is summarized in Table 8. Before the load P_c , the steel wire is in the elastic stage. Even if the crack of the concrete at the crown/invert inner surface reaches 0.25 mm, the steel wire is still in the elastic stage. The steel wire reaches the elastic limit state until there are visible cracks in the mortar at the springing line. At $1.6 P_c$, the stress of the steel wire on some zones is close to the yield strength, which means that the wire reaches the strength limit state. When the concrete at the PCCP crown/invert zones cracks, the springing line of the PCCP will be subjected to additional tensile stress due to the effect of moment redistribution [11]. When the concrete crack width exceeds 0.25 mm, the steel wire rapidly reaches the elastic limit state and thereby yields. The cracking of the concrete at the crown/invert zones will accelerate the damage of the steel wire at the springing line. Therefore, delaying the extension of concrete cracks at the crown/invert zones contributes to the protection of prestressed steel wires.

Table 8. Stress state of prestressed steel wire at the springing line at different stages.

Pipe Condition	Load	Max. Strain ($\mu\epsilon$)	Max. Stress (MPa)	Actual Stress (Mpa)	Wire Condition
Microcracking on inner concrete at crown/invert	P_c	232	48	993	Elastic
Visible cracking on inner concrete at crown/invert	$1.1 P_c$	278	57	1002	Elastic
Concrete cracks with width of 0.25 mm	$1.3 P_c$	421	87	1032	Elastic
Visible cracking on mortar at the springing line	$1.5 P_c$	869	178	1123	Elastic limit
Visible cracking on outer concrete at the springing line	$1.6 P_c$	1199	229	1174	Strength limit

5.3. Cracking Load for Mortar

The strain and corresponding load at the characteristic points of the mortar on the springing line are shown in Table 9, where the multiple value of the control strain at the theoretical cracking point can be obtained according to the following derivation process:

Table 9. Corresponding loads of mortar in different states at the springing line.

Stage	Strain ($\mu\epsilon$)	Strain Multiple	Test Load (P_c)
Elastic limit	144	/	0.6
Theoretically cracking point	576	4	1.2~1.3
Micro cracking	922	6.4	1.4
Visible cracking	1152	8	1.4~1.5

The strain of the mortar in the process of pipe loading can be divided into before and after the decompression point of the pipe's core concrete. Since the mortar is not prestressed, the mortar and concrete deform together before the decompression point, resulting in strain ϵ_{m1} . When the decompression point is reached, the mortar strain will produce the second part of the strain ϵ_{m2} due to the concrete having no prestress. The total strain of the protective mortar is found in the compression process $\epsilon_m = \epsilon_{m1} + \epsilon_{m2}$, which

can be calculated according to Formula (5), of which the loss of the modulus of elasticity of the mortar in the softening stage was neglected [37].

$$\epsilon_m = \frac{0.5 \times 0.7 f_{cu,k}}{E_c} + \frac{\alpha n_m f_{tk}}{7713 (f_{mc,k})^{0.3}} \tag{5}$$

where $f_{cu,k}$ is the standard value of cubic compressive strength, Mpa; E_m is the modulus of elastic, Mpa; $f_{mc,k}$ is the standard value of cubic compressive strength, Mpa.

The value of ϵ_m is 624 $\mu\epsilon$ as calculated by Formula (5). According to Table 5, ϵ_{me} is 144 $\mu\epsilon$. The ratio of ϵ_m and ϵ_{me} is 4.3. Hence, the theoretical cracking point is 4 ϵ_{me} . Combined with the test and theoretical analysis, the mortar is in the elastic stage before 0.6 P_c , reaches the theoretical cracking point at 1.2 P_c and exhibits visible cracking after 1.4 P_c .

The effect of moment redistribution leads to an increase in tensile stress on the protective mortar at the springing line. This results in the cracks on the protective mortar when the prestressed steel reaches the elastic limit state. Therefore, delaying the cracking of concrete at the crown/invert zones of PCCP benefits the prevention of cracking of the protective mortar at the springing line.

5.4. Mechanical Response of PCCP under Overload Condition

The deformation stages of the pipe under external load are shown in Figure 16. The test results show that the tested PCCP meets the inspection provisions within the P_c range specified in code GB/T 19,685 [2]. The concrete of the crown and invert zones of the pipe’s inner surface reach the serviceability limit state at 1.1 P_c , and the concrete and mortar at the springing line reach the serviceability limit state at 1.5 P_c . The prestressed steel wire reaches the elastic limit state at 1.5 P_c and the strength limit state at 1.6 P_c . The design method of code CECS 140 [14] calculates the internal elastic force of the pipe. When the pipe reaches the serviceability limit state, the concrete is not considered to participate in the force, and the maximum bearing capacity at the springing line is borne by the steel wire. The results show that the ultimate failure load of the tested PCCP is greater than 1.6 P_c , and there is sufficient safety in actual operation.

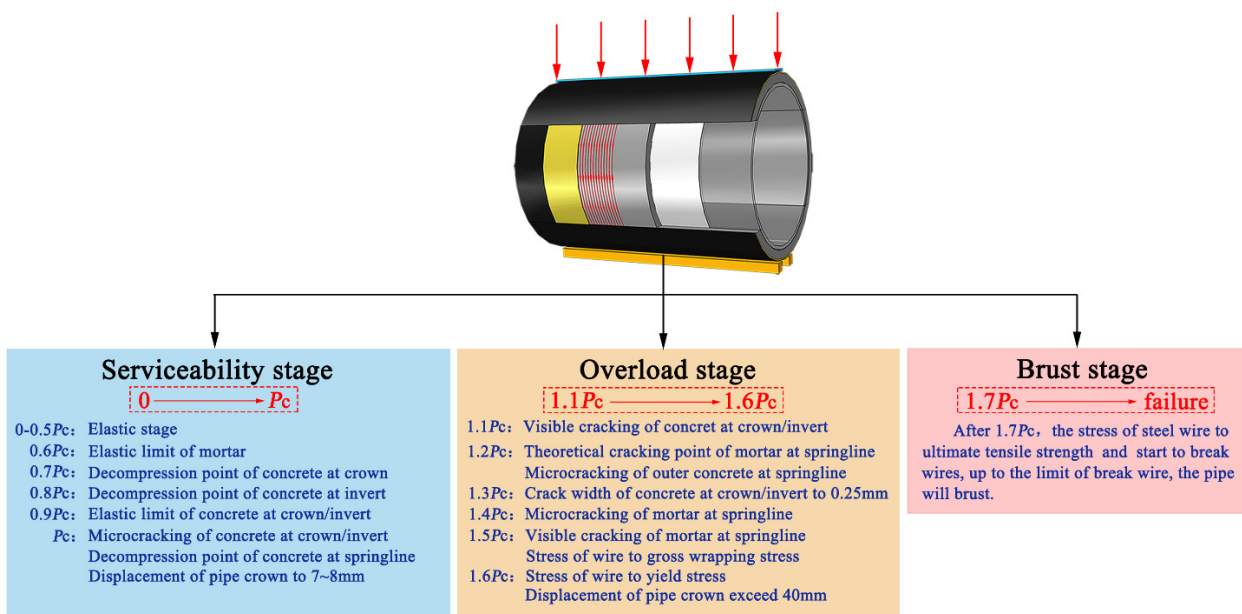


Figure 16. Schematic diagram of PCCP mechanical response.

6. Conclusions

In this paper, the prototype test of the embedded PCCP with a pipe diameter of 3.2 m is carried out in combination with practical engineering. Based on the test results, the conclusions are as follows:

(1) Under external load, the cracking of the pipe's crown occurred earlier than that of the invert. The cracking on the crown zone occurred earlier than that on the invert zone of the pipe. When loading to 130% P_c , cracks at the crown and invert of the pipe are connected and the width of the cracks exceeds 0.25 mm. The difference comes from the support conditions at the invert and the loading method on the crown.

(2) With the load up to P_c , the inner wall concrete at the crown of the pipe first reaches the visible crack control strain. With the load up to 1.1 P_c , the strain of the concrete at the springing line is below 300 $\mu\epsilon$ due to the existence of prestressing, while the visible cracks appear on the crown/invert zones of the inside concrete. The final strain of the inside concrete at the springing line is lower than that at the outside concrete. The control strain of visible cracking in code AWWA C304 is specified as 11 ϵ_{ce} (1082 $\mu\epsilon$), which is higher than the 9.5 ϵ_{ce} (970 $\mu\epsilon$) monitored in this test. The actual cracking load (1.1 P_c) is slightly higher than the calculated load (P_c).

(3) Before the load reaches 1.3 P_c , the steel wire is in the elastic stage. When the concrete crack width exceeds 0.25 mm after 1.3 P_c , the steel wire rapidly reaches the elastic limit state. After the load reaches 1.6 P_c , the strength of the prestressed steel wire is close to the yield strength and subsequently reaches the strength limit state.

(4) When the concrete at the PCCP's crown/invert zones cracks, the springing line of PCCP will endure additional tensile stress due to the effect of moment redistribution. This leads to the cracking of the protective mortar at the load 1.2 P_c . Therefore, delaying the extension of concrete cracks at the crown/invert zones has a positive effect on the protection of the prestressed steel wires along the springing line.

(5) The PCCP designed by the limit state design method can resist external loads after reaching the serviceability limit state. The results show that the ultimate failure load of the tested PCCP is greater than 1.6 P_c , and there is sufficient safety in actual operation.

However, the damage on the concrete at the crown/invert zones will become a fuse of PCCP failure. In this aspect, more attention should be paid to improving the tensile resistance used for PCCP. This also benefits the durability improvement of PCCP in corrosive environments.

Author Contributions: Conceptualization, P.S. and S.Z.; methodology, H.W. and S.Z.; validation, P.S. and F.Q.; formal analysis, D.Z.; investigation, D.Z. and W.Z.; data curation, P.S.; writing—original draft preparation, P.S.; writing—review and editing, P.S. and S.Z.; visualization, P.S. and H.W.; supervision, S.Z. and F.Q.; funding acquisition, P.S. and F.Q. All authors have read and agreed to the published version of the manuscript.

Funding: This research was funded by the Key R&D projects in Henan Province, grant number 202102310250; the Doctoral Innovation Foundation of North China University of Water Resources and Electric Power, grant number HSZ2021-252; and National Key Engineering Project of Pipe Procurement for Yangtze River to Huaihe River (Henan section), grant number FCGY/JC2020/001.

Institutional Review Board Statement: Not applicable.

Informed Consent Statement: Not applicable.

Data Availability Statement: Data are available with the first author and can be shared with anyone upon reasonable request.

Conflicts of Interest: The authors declare no conflict of interest.

References

1. Kennison, H.F. Design of prestressed concrete cylinder pipe. *J. (Am. Water Work. Assoc.)* **1950**, *42*, 1049–1064. [[CrossRef](#)]
2. *GB/T 19685-2017*; Prestressed Concrete Cylinder Pipe. China Standards Press: Beijing, China, 2017.

3. ANSI/AWWA C304–2014; AWWA Standard for Design of Prestressed Concrete Pressure Pipe. American National Standards Institute; American Water Works Association: New York, NY, USA; Denver, CO, USA, 2014.
4. Ge, S.Q.; Sinha, S. Failure analysis, condition assessment technologies, and performance prediction of prestressed-concrete cylinder pipe: State-of-the-art literature review. *J. Perform. Constr. Facil.* **2012**, *28*, 618–628. [[CrossRef](#)]
5. Hu, B.Y. Study on Service Performance of Prestressed Concrete Cylinder Pipe with Broken Wires. Master's Thesis, Zhengzhou University, Zhengzhou, China, 2020.
6. Lee, Y.; Lee, E.T. Retrofit design of damaged prestressed concrete cylinder pipes. *Int. J. Concrete. Struct. Mater.* **2013**, *7*, 265–271. [[CrossRef](#)]
7. Hu, S.W.; Shen, J.; Wang, D.L.; Cai, X. Experiment and numerical analysis on super caliber prestressed concrete cylinder pipes with cracks. *J. Hydraul. Eng.* **2010**, *41*, 876–882.
8. Zhai, K.J.; Fang, H.Y.; Guo, C.C.; Ni, P.P.; Wu, H.Y.; Wang, F.M. Full-scale experiment and numerical simulation of prestressed concrete cylinder pipe with broken wires strengthened by prestressed CFRP. *Tunn. Undergr. Space Technol.* **2021**, *115*, 104021. [[CrossRef](#)]
9. ANSI/AWWA C301–1984; AWWA Standard for Prestressed Concrete Pressure Pipe, Steel Cylinder Type, for Water and Other Liquids. American Water Works Association: Denver, CO, USA, 1984.
10. Zarghamee, M.S.; Heger, F.J.; Dana, W.R. Experimental evaluation of design methods for prestressed concrete pipe. *J. Transp. Eng.* **1988**, *114*, 635–655. [[CrossRef](#)]
11. Zarghamee, M.S.; Fok, K.L. Analysis of prestressed concrete pipe under combined loads. *J. Struct. Eng.* **1990**, *116*, 2022–2039. [[CrossRef](#)]
12. Heger, F.J.; Zarghamee, M.S.; Dana, W.R. Limit-states design of prestressed concrete pipe. I: Criteria. *J. Struct. Eng.* **1990**, *116*, 2083–2104. [[CrossRef](#)]
13. Zarghamee, M.S.; Fok, K.L.; Sikiotis, E.S. Limit-states design of prestressed concrete pipe. II: Procedure. *J. Struct. Eng.* **1990**, *116*, 2105–2126.
14. CECS 140-2011; Specification for Structural Design of Buried Prestressed Concrete Pipeline and Prestressed Concrete Cylinder Pipeline of Water Supply and Sewerage Engineering. China Planning Press: Beijing, China, 2011.
15. SL 702-2015; Technical Specifications of Prestressed Concrete Cylinder Pipe. China Waterpower Press: Beijing, China, 2015.
16. Hu, S.W.; Shen, J.; Wang, D.L.; Liu, X.X. External load test on super-diameter concrete cylinder pipe (PCCP) in Mid-route of South-to-North Water Transfer Project. *Water. Res. Hydrop. Eng.* **2009**, *40*, 31–33.
17. Dou, T.S.; Cheng, B.Q.; Hu, H.; Xia, S.F.; Yang, J.X.; Zhang, Q. The prototype test study of prestressed concrete cylinder pipe structure deformation law II: The external pressure. *J. Hydraul. Eng.* **2018**, *49*, 207–215.
18. Chen, B.Q.; Dou, T.S.; Xia, S.F. Experimental study on mechanical properties of prestressed concrete cylinder pipes (PCCPs) under external load. *Int. J. Pres. Ves. Pip.* **2021**, *191*, 104365. [[CrossRef](#)]
19. Zhao, X.L.; Dou, T.S.; Yan, J.Q.; Wang, R.L. Experimental Study on the Bearing Capacity of PCCP Pipe with Longitudinal Cracks on the Outside of the Pipe Core. *China. Concr. Cem. Prod.* **2012**, *12*, 37–40.
20. Dong, X.N.; Dou, T.S.; Cheng, B.Q.; Zhao, L.J. Failure analysis of a prestressed concrete cylinder pipe under clustered broken wires by FEM. *Structures* **2021**, *33*, 3284–3297. [[CrossRef](#)]
21. Zhai, K.J.; Wang, F.M.; Fang, H.Y.; Ni, P.P.; Ji, X.B.; Guo, C.C.; Hu, S.W. Serviceability assessment of prestressed concrete cylinder pipes with broken wires: Analytical solution and numerical simulation. *Tunn. Undergr. Space Technol.* **2022**, *126*, 104551. [[CrossRef](#)]
22. Zhai, K.J.; Fang, H.Y.; Guo, C.C.; Fu, B.; Ni, P.P.; Ma, H.H.; He, H.; Wang, F.M. Mechanical properties of CFRP-strengthened prestressed concrete cylinder pipe based on multi-field coupling. *Thin. Wall. Struct.* **2021**, *162*, 107629. [[CrossRef](#)]
23. Wardany, R.A. Condition assessment of prestressed concrete cylindrical water pipes. In Proceedings of the 60th Annual WCWWA Conference and Trade Show, Western Canada Water and Wastewater Association, Cochrane, AB, Canada, 23–26 September 2008; pp. 1–9.
24. Wang, X.; Hu, S.W.; Li, W.H.; Hu, Y.Q. Corrosion monitoring for prestressed concrete cylinder pipe spigot with combined use of Tafel extrapolation and surface acoustic wave methods. *Constr. Build. Mater.* **2022**, *337*, 127572. [[CrossRef](#)]
25. Li, H.Z.; Feng, X.; Zhao, L. Failure analysis of a buried large-diameter prestressed concrete cylinder pipeline subjected to strike-slip fault displacement. *Tunn. Undergr. Space Technol.* **2022**, *121*, 104334. [[CrossRef](#)]
26. Wu, H.Y.; Zhai, K.J.; Fang, H.Y.; Wang, F.M.; Yu, L.; Li, B. Bell-and-spigot joints mechanical properties study of PCCP under the uneven settlement of foundation Simulation and full-scale test. *Structures* **2022**, *43*, 1692–1703. [[CrossRef](#)]
27. Hassi, S.; Ejbouh, A.; Touhami, M.E.; Berrami, K.; Ech-chebab, A.; Boujad, A. Performance of Prestressed Concrete Cylinder Pipe in North Africa: Case Study of the Water Transmission Systems in the Tafilalet Region of Morocco. *J. Pipeline Syst. Eng. Pract.* **2021**, *12*, 05021002. [[CrossRef](#)]
28. Berrami, K.; Ech-chebab, A.; Galai, M.; Ejbouh, A.; Hassi, S.; Benqlilou, H.; Ouaki, B.; Ebn Touhami, M. Evaluation of fly ash effect on the durability of prestressed concrete cylindrical pipe in aggressive soil by electrochemical method. *Chem. Data. Collect.* **2021**, *32*, 100656. [[CrossRef](#)]
29. Ejbouh, A.; Ech-chebab, A.; Galai, M.; Lachhab, R.; Benqlilou, H.; Touhami, M.E. Effects of fly ash and simulation of the natural hot and dry climate of the Moroccan desert region on the durability of prestressed concrete cylinder pipes. *J. Pipeline Syst. Eng. Pract.* **2022**, *13*, 04022029. [[CrossRef](#)]

30. Ge, S.; Sinha, S. Effect of various bedding conditions on structural integrity of prestressed concrete cylinder pipe. *J. Mater. Sci. Res.* **2015**, *4*, 34. [[CrossRef](#)]
31. *ANSI/AWWA C301–2014*; AWWA Standard for Prestressed Concrete Pressure Pipe, Steel-Cylinder Type. American National Standards Institute: New York, NY, USA; American Water Works Association: Denver, CO, USA, 2014.
32. *GB 50010-2010 (version 2015)*; Code for Design of Concrete Structures. China Building Industry Press: Beijing, China, 2015.
33. *GB 50017-2017*; Standard for Design of Steel Structures. China Building Industry Press: Beijing, China, 2017.
34. *GB/T 5223-2014*; Steel Wire for Prestressing of Concrete. China Standards Press: Beijing, China, 2014.
35. *GB/T 15345-2017*; Test Methods of Concrete Pipes for Water Transmission. China Standards Press: Beijing, China, 2017.
36. *ASTM C497-2019*; Standard Test Methods for Concrete Pipe, Concrete Box Sections, Manhole Sections, or Tile. American Society of Testing Materials: West Conshohocken, PA, USA, 2019.
37. Que, X.P. Understandings of internal and external pressure test load formulas of PCCP of GB/T19685—2005 prestressed concrete steel cylinder pipe. *China Concr. Cem. Prod.* **2014**, *2*, 23–26.